Amplified Inception of European Little Ice Age by Sea Ice–Ocean–Atmosphere Feedbacks

FLAVIO LEHNER, ANDREAS BORN, CHRISTOPH C. RAIBLE, AND THOMAS F. STOCKER

Climate and Environmental Physics and Oeschger Centre for Climate Change Research, University of Bern, Bern, Switzerland

(Manuscript received 26 September 2012, in final form 21 March 2013)

ABSTRACT

The inception of the Little Ice Age (~1400–1700 AD) is believed to have been driven by an interplay of external forcing and climate system internal variability. While the hemispheric signal seems to have been dominated by solar irradiance and volcanic eruptions, the understanding of mechanisms shaping the climate on a continental scale is less robust. In an ensemble of transient model simulations and a new type of sensitivity experiments with artificial sea ice growth, the authors identify a sea ice–ocean–atmosphere feedback mechanism that amplifies the Little Ice Age cooling in the North Atlantic–European region and produces the temperature pattern suggested by paleoclimatic reconstructions. Initiated by increasing negative forcing, the Arctic sea ice substantially expands at the beginning of the Little Ice Age. The excess of sea ice is exported to the subpolar North Atlantic, where it melts, thereby weakening convection of the ocean. Consequently, northward ocean heat transport is reduced, reinforcing the expansion of the sea ice and the cooling of the Northern Hemisphere. In the Nordic Seas, sea surface height anomalies cause the oceanic recirculation to strengthen at the expense of the warm Barents Sea inflow, thereby further reinforcing sea ice growth. The absent ocean–atmosphere heat flux in the Barents Sea results in an amplified cooling over Northern Europe. The positive nature of this feedback mechanism enables sea ice to remain in an expanded state for decades up to a century, favoring sustained cold periods over Europe such as the Little Ice Age. Support for the feedback mechanism comes from recent proxy reconstructions around the Nordic Seas.

1. Introduction

The past 1000 years are a prime target for studies of internal variability of the climate system because of the relatively weak orbital and solar forcing and the abundance of climate proxy reconstructions. The most prominent departures from the mean climate trend during that time were the Medieval Climate Anomaly (MCA) from ~950 to 1250 AD, a relatively warm period with stronger solar irradiance, and the subsequent Little Ice Age (LIA) from ~1400 to 1700 AD, a cooling period of reduced solar irradiance and increased volcanic activity (Mann et al. 2009). Cooling from early anthropogenic land cover changes is negligible before 1500 AD (e.g., Bauer et al. 2003). While the global signal of the MCA–LIA transition is attributed to the changes in external forcing of solar irradiance and volcanic eruptions, climate variations on continental scales are less understood (Wanner et al. 2008, and references therein). Temperature reconstructions suggest that the cooling of the LIA was neither spatially nor temporally uniform (e.g., Matthews and Briffa 2005; Wanner et al. 2011). Thus, feedback mechanisms within the climate system are necessary to explain this heterogeneity. In Europe, for example, the reconstructed cooling during the LIA was strongest in the north, while it was weaker toward the south (Mann et al. 2009). This has been interpreted as a fingerprint of a shift from a persistent positive to a negative North Atlantic Oscillation (NAO) (Trouet et al. 2009), but the robustness of this NAO reconstruction remains questionable (Lehner et al. 2012a; Pinto and Raible 2012).

The apparent difficulties of relating the MCA–LIA transition to fundamental changes in the leading mode of atmospheric winter variability opens the opportunity for alternative mechanisms that also employ other components of the climate system, namely, the ocean or sea ice. Zhong et al. (2011) forced a climate model with a series of decadally paced volcanic eruptions, while leaving solar irradiance constantly at 1000 AD levels. They found a sea ice–ocean feedback loop that allows Arctic sea ice cover to remain in an extended state and

Corresponding author address: Flavio Lehner, Climate and Environmental Physics, University of Bern Sidlerstrasse 5, CH-3012 Bern, Switzerland.
E-mail: lehner@climate.unibe.ch

DOI: 10.1175/JCLI-D-12-00690.1

cool the Northern Hemisphere for decades after the last volcanic eruptions. Based on these findings, Miller et al. (2012) proposed a volcanic trigger for the onset of the LIA in the North Atlantic–European region.

Abrupt climate shifts in the absence of strong forcing changes (e.g., the occurrence of the LIA) have been identified in observations and climate models before. Using a long and unforced climate model simulation, Goosse and Renssen (2002) describe events of spontaneous weakening of convection in the Nordic Seas that cause century-long hemispheric and Arctic cooling. Similar cooling events in a climate model forced with slightly varying solar irradiance were attributed to a shutdown of the Barents Sea inflow (Semenov et al. 2009), a crucial transport branch of warm and salty Atlantic waters into the Arctic (Ingvaldsen et al. 2004). In the context of twentieth-century warming events in the Arctic, many studies suggest that the Barents Sea inflow, if strengthened, can explain part of the warming and the corresponding sea ice retreat (e.g., Bengtsson et al. 2004; Årthun et al. 2012). While the Barents Sea inflow is driven partly by regional winds (Ingvaldsen et al. 2004), its strengths and composition are also remotely forced by advection of North Atlantic thermohaline properties (Holliday et al. 2008). The advection of these properties, in turn, depends largely on the strength of the broader-scale North Atlantic circulation, described by the Atlantic meridional overturning circulation (AMOC). New proxy evidence from the North Atlantic and adjacent basins points toward the AMOC and associated ocean currents having played an amplifying role in the MCA–LIA transition (Spielhagen et al. 2011; Hald et al. 2011; Wanamaker et al. 2012; Kuhnert and Mulitza 2011).

The aim of this study is to investigate the role of the Barents Sea inflow and the associated sea ice–ocean–atmosphere coupling at the inception of the LIA in the North Atlantic–European region. To that end, we use transient model simulations covering the transitional period from 1150 to 1500 AD. While the coolest period of the European LIA was around 1650–1700 AD, roughly 70% of the European cooling since the MCA occurred before 1500 AD, as reconstructions by Mann et al. (2009) illustrate. Additionally, we conduct sensitivity experiments in which sea ice is artificially grown in the Barents and the Labrador Sea to investigate feedbacks potentially associated with the MCA–LIA transition. The latter experiments are, to our knowledge, a novelty in coupled modeling and provide useful new insights on the dynamics of sea ice–ocean interaction. They are also a new tool in the context of paleoclimatology, as the few existing experiments that introduced sea ice perturbations in a coupled model mainly focus on future climate change: by sudden removal of the Arctic sea ice (Schröder and Connolley 2007; Tietsche et al. 2011) or by tuning the ice albedo (Bitz et al. 2006; Holland et al. 2006) the resilience of sea ice to projected warming has been investigated.

This paper is structured as follows: A description of the model and experimental setup is presented in section 2. In sections 3 and 4 the transient and the sensitivity experiments are examined, with a focus on feedbacks within the climate system. A discussion and conclusions follow in section 5.

2. Data and methods

a. Model description

We use the Community Climate System Model 3 (CCSM3) provided by the National Center for Atmospheric Research (NCAR) (Collins et al. 2006). It is a coupled model with atmosphere, ocean, sea ice, and land surface components all communicating through a coupler without flux correction. The CCSM3 has been used in various studies addressing questions of paleoclimate (e.g., Liu et al. 2009; Yoshimori et al. 2010; Hofer et al. 2011, 2012a,b; Lehner et al. 2012a,b; Wilmes et al. 2012), present-day and future climate (e.g., Meehl et al. 2006), as well as in sensitivity experiments applying freshwater hosing (e.g., Stocker et al. 2007) or idealized CO_2 increase (e.g., Bryan et al. 2006). We use the intermediate resolution version of CCSM3 (Otto-Bliesner et al. 2006). The atmosphere and land surface components are truncated at T42, resulting in a horizontal resolution of approximately $2.8° \times 2.8°$; the atmosphere has 26 levels reaching up to 8.3 hPa. The ocean and sea ice components both operate on a nominal 1° resolution grid; however, the displacement of the North Pole into Greenland allows for a higher resolution in the Arctic and an open passage through the Canadian Arctic Archipelago. The ocean component has a maximum of 40 levels at depth. The sea ice component is the Community Sea Ice Model (CSIM), applying elastic–viscous–plastic dynamics and thermodynamics.

b. Control simulation

An overview of the simulations conducted for this study is given in Table 1. The control simulation (CTRL) is an equilibrium simulation using constant values in 1150 AD for total solar irradiance (TSI, 1366.4 $W m^{-2}$), CO_2 (283.9 ppm), CH_4 (704.9 ppb), and N_2O (265.0 ppb). CTRL is a branch from the preindustrial simulation (perpetual 1870 AD conditions) described by Otto-Bliesner et al. (2006). Despite representing the relatively warm climate of the Medieval Climate Anomaly

TABLE 1. List of all simulations and number of runs (N).

Name	Description	Length (N)
CTRL	1150 AD equilibrium simulation	494 yr (1)
TR1–TR6	Transient simulation (1150–1500 AD)	351 yr (6)
TR_novolc	Transient simulation (1150–1500 AD) but without volcanoes	351 yr (1)
BSf25	Sea ice growth enhanced by a factor $f' = 25$ in Barents Sea for 100 yr, then switched off artificial growth	200 yr (1)
LSf25	Sea ice growth enhanced by a factor $f' = 25$ in Labrador Sea for 100 yr, then switched off artificial growth	200 yr (1)

(as compared to the almost-linear orbital cooling trend over the last millennium), Northern Hemisphere winter (November–April) temperature in the CTRL is on average 2.6°C lower than in a 1990 control simulation with the same model, owing primarily to substantially lower greenhouse gas concentrations. This results in sea ice concentrations being larger than today in most locations of the Northern Hemisphere. During winter large parts of the Barents and Labrador Seas are covered by sea ice > 15% (Fig. 1a). Both seasonal and interannual variability is largest in the Barents Sea. There, most of the newly formed winter sea ice is exported northward to the Arctic Ocean. At the same time, the sea ice cover is sensitive to interannual variations in the inflow of warm Atlantic waters, characterizing the Barents Sea as a key region in the Arctic–North Atlantic freshwater cycle. The atmospheric winter circulation in the North Atlantic–European area is dominated by the well-known North Atlantic Oscillation (NAO) pattern, featuring a low pressure system just south of Iceland and a high pressure system over the Azores (Fig. 1b). The cyclonic circulation of the northern center of action transports heat northward on its eastern side, thereby contributing to the comparably mild climate of Northern Europe. The largest interannual variability in SLP occurs to the northwest of this low pressure system resembling the nonstationary northern center of action of the NAO (Fig. 1b).

c. *Transient simulations*

The transient simulations (TR1–TR6) were branched from different initial conditions of CTRL applying the same time-varying external forcing of total solar irradiance, greenhouse gases, and volcanic eruptions for the period 1150–1500 AD (the forcings used are as described in Yoshimori et al. 2010). Compared to the bulk of recent TSI reconstructions (for an overview, see Schmidt et al. 2012), our TSI has a relatively large amplitude of approximately 2.3 W m^{-2} from the MCA (in this study defined as 1150–1200 AD) to the LIA

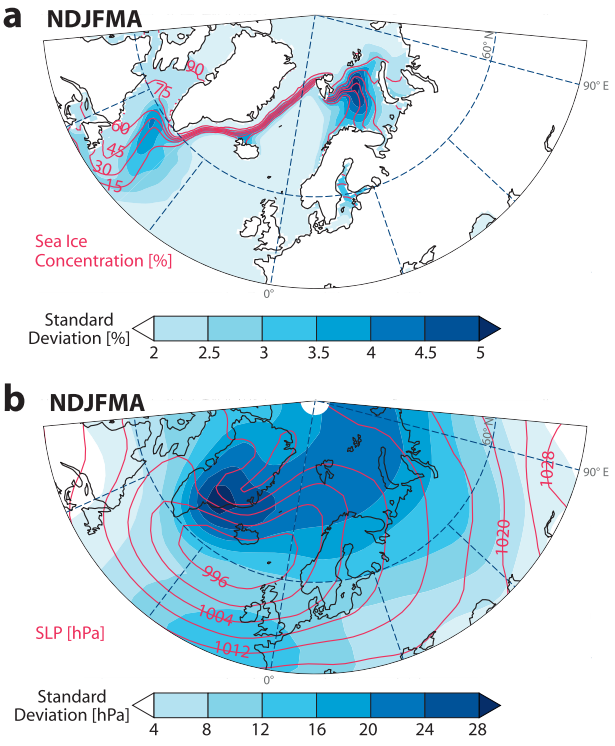

FIG. 1. Long-term winter (November–April) mean and standard deviation from CTRL (494 yr) for (a) sea ice concentration and (b) sea level pressure (SLP).

(1450–1500 AD).[1] The forcings and their radiative effect are shown in Figs. 2a,b. In these forcing datasets the time around 1150 AD marks the beginning of a decrease in TSI: that is, the inception of the Little Ice Age. This is reflected in a decreased Northern Hemisphere temperature and an increased Arctic sea ice extent (Figs. 2c,d), two features well reproduced by the model when compared with proxies (Solomon et al. 2007; Kinnard et al. 2011). However, the minimum and maximum of both temperature and sea ice fall just within the uncertainty of the reconstructions, although the applied solar forcing is relatively strong. In the following, the term ''negative forcing'' is used when the decrease in TSI from MCA to LIA and the radiative cooling from volcanoes are addressed in an integral manner. The initial conditions for the different transient simulations were selected to cover a range of states of the Atlantic meridional overturning circulation (AMOC), as the North Atlantic, European, and Arctic climate is substantially influenced by the strength of the AMOC (e.g., Hofer et al. 2011). In the following

[1] For comparison with other studies, the TSI amplitude from the Maunder Minimum to the period 1950–2000 AD is 3.3 W m^{-2}.

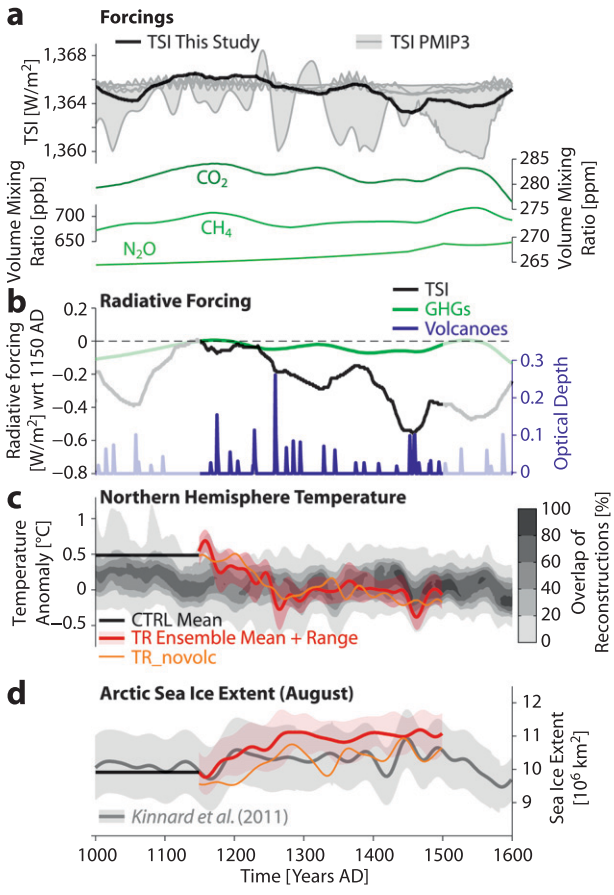

FIG. 2. (a) Forcing used in the model simulations which cover the time period 1150–1500 AD: TSI used in this study and from the protocol of the third Paleoclimate Modeling Intercomparison Project (Schmidt et al. 2012); changes in greenhouse gases (GHGs: CO_2, CH_4, N_2O). (b) Cumulative radiative forcing from GHGs (calculated as in Houghton et al. 2001) and TSI (assuming a global average albedo of 0.31), with respect to (wrt) 1150 AD and changes in the annual mean visible band optical depth due to volcanic eruptions. (c) Northern Hemisphere annual mean temperature anomaly from reconstructions (gray shading; Fig. 6.13d in Solomon et al. 2007) and the model simulations (30-yr Fourier filtered). The reconstructions are wrt 1500–1899 AD. As the simulations do not cover that time period, they are adjusted to have the same mean as the reconstructions time series during the overlapping time period, that is, from 1150 to 1500 AD. (d) August Arctic sea ice extent (sea ice concentration $> 15\%$) from the reconstruction of Kinnard et al. (2011) and the model simulations (80-yr Fourier filtered).

sections, we refer to the ensemble mean of TR1–TR6 as the transient simulations. Further, one of the transient simulations was rerun without volcanic eruptions (TR_novolc) to determine the impact of variations in TSI and greenhouse gases only.

When comparing with proxy reconstructions at coarse temporal resolution, a low-pass Fourier filter is applied to the model time series. After transformation of the time series to the frequency domain, frequencies above the frequency $\nu_0 > 1/T$ are set to zero, where T is the cutoff period (30, 40, and 80 yr, respectively). To reduce Gibbs phenomenon artifacts from a sharp cutoff, we use a smooth transition phase (rolloff) between $\nu = \nu_0 \pm \nu_0/2$.

d. Artificial sea ice growth simulations

In addition to the transient ensemble, two 200-yr-long sensitivity experiments were branched from CTRL in which perpetual 1150 AD conditions apply, but sea ice growth in the Barents Sea (experiment called BSf25) and Labrador Sea (LSf25) was artificially enhanced by a factor of 25 for the first 100 years (Fig. 3a and Table 1). The regions of artificially enhanced sea ice growth were chosen for their distinct roles in the freshwater cycle of the Arctic–North Atlantic area: the Labrador Sea imports sea ice that melts locally, whereas the Barents Sea rather acts as a source of sea ice, especially in colder climates such as the LIA. By enhancing sea ice growth in LSf25 experiment, we transform this region into a sea ice source. Thereby, we directly increase the amount of sea ice in a region crucial for deep-water formation (Bryan et al. 2006), aiming for a relatively rapid response of the AMOC. This makes LSf25 comparable to classical freshwater hosing experiments, which are often set in a similar location. In BSf25 experiment, on the other hand, we only enhance the natural role this basin plays in the freshwater cycle.

Frazil ice is the first stage of ice growth, resulting from strong heat loss over areas of open water:

$$V_{\text{frazil}} = -\rho_{\text{ice}}^{-1}\frac{Q}{H} f' A \Delta t, \qquad (1)$$

where V_{frazil} is the volume of new ice added to the first ice category (i.e., frazil ice), Q is the heat flux to open water for this new ice, H is enthalpy for new ice, f' is the perturbation factor introduced (25 in this study), Δt is the model time step, ρ_{ice} the density of ice, and A the area of sea ice growth. By enhancing growth only for frazil ice, the direct disturbance is minimal as the model dynamics remain unchanged. The model retains the freedom to melt and redistribute the additional frazil ice, change its mechanical characteristics by mixing with other ice categories, and form congelation ice on the newly formed ice cover in the subsequent growth seasons. Note that, by multiplying the model-derived heat flux, the seasonality of ice growth as well as the distribution of newly formed ice remains consistent in the coupled system. In contrast to other studies, the additional sea ice is not added at once or prescribed as lower boundary condition (e.g., Petoukhov and Semenov 2010; Li et al. 2010).

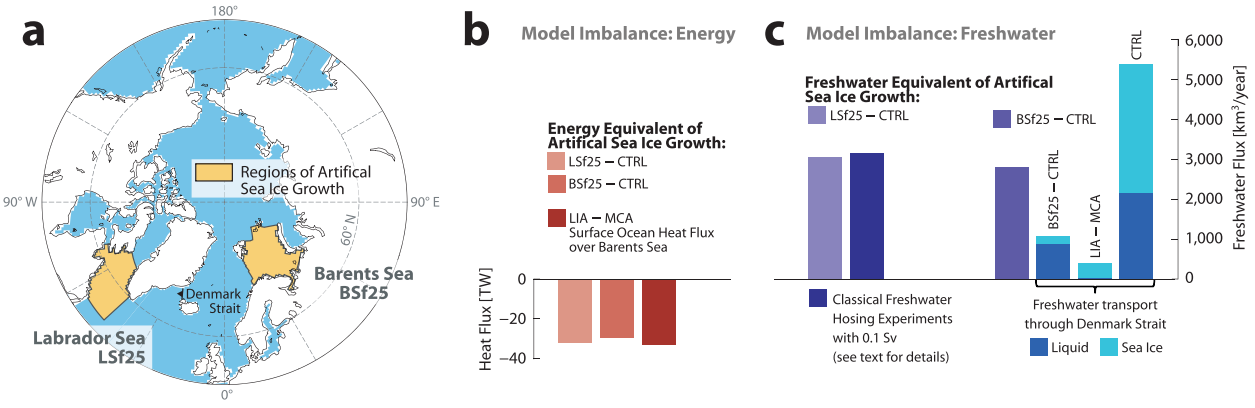

FIG. 3. (a) Map of the Arctic with the regions of artificial sea ice growth. (b) Estimates of the model imbalance in energy; shown are average anomalies of the first 100 yr of BSf25 and LSf25 from the CTRL and the LIA − MCA difference in ocean–atmosphere heat flux over the Barents Sea. (c) Estimates of the model imbalance in freshwater; shown are average anomalies of the first 100 yr of BSf25 and LSf25 from the CTRL mean. For comparison with the LSf25 experiment, the amount of freshwater put into the subpolar North Atlantic in classical freshwater hosing experiments is given. For comparison with the BSf25 experiment, the annual freshwater transport through the Denmark Strait [see map in (a) for location] is given for BSf25 (first 100 yr)–CTRL mean, LIA–MCA, and CTRL mean. Liquid freshwater transports are calculated to a reference salinity of 34.7 (see text for further details).

Owing to the modification of the sea ice code, freshwater and heat are not conserved in these experiments (Figs. 3b,c). The brine rejection by frazil ice growth is calculated in the ocean component and does not take into account the perturbation factor f', which is only applied in the ice component. Therefore, brine rejection is underestimated, making the model fresher wherever additional sea ice melts. Along the same lines, when the additional sea ice melts (anywhere in the ocean), it will consume heat from the ocean that has not been introduced into the ocean before because the air–sea heat flux Q is not changed. This eventually makes the model colder on a global scale. However, by design of the sea ice perturbation, no imbalances are introduced locally in the forcing regions. Heat and freshwater flux anomalies there are the result of reactions of the coupled climate system to the anomalous forcing, as intended for the present study. This makes it impossible to determine the exact location of occurring imbalances, which is also why we refrain from any flux adjustments to compensate.

To put these imbalances into context, we compare them to other processes. Figure 3b shows the energy equivalent of the anomalous annual frazil ice growth. This is estimated from the difference in 100-yr cumulative frazil ice growth between the two sensitivity experiments and CTRL (for CTRL the average over four 100-yr segments is used) multiplied by the specific heat capacity of ice. The two sensitivity experiments extract a similar amount of energy from the system (around 30 TW), which is comparable to the reduction in ocean–atmosphere heat flux over the Barents Sea in the transient simulations. If we reintroduced this energy in situ, most of it would instantly radiate to the atmosphere, as during winter sea surface temperatures usually exceed air temperatures in the Barents Sea (not shown). This would disturb the lower atmosphere, similar to artificial sea ice growth via changes in albedo, which is another reason to refrain from flux adjustment.

Figure 3c shows the imbalance in freshwater for the two sensitivity experiments, derived from the average anomalous annual frazil ice growth, which is 3035 $\mathrm{km^3\,yr^{-1}}$ in LSf25 and 2783 $\mathrm{km^3\,yr^{-1}}$ in BSf25 (Fig. 3c). Over the 100 years of the artificial sea ice growth, this translates into additional frazil ice volume of about $300 \times 10^3\,\mathrm{km^3}$ and $280 \times 10^3\,\mathrm{km^3}$, respectively. The amount of additional freshwater delivered to the system in LSf25 is reminiscent of freshwater amounts deployed into the subpolar North Atlantic in classical hosing experiments (e.g., Stouffer et al. 2006; Stocker et al. 2007). There, hosing with 0.1 Sv ($\mathrm{Sv} \equiv 10^6\,\mathrm{m^3\,s^{-1}}$) (3154 $\mathrm{km^3\,yr^{-1}}$) triggers an AMOC reduction of about 4 Sv, which is comparable to the 2–3-Sv reduction that occurs in our transient simulations (see section 3). In LSf25 most of the artificially grown sea ice melts in situ or in the subpolar North Atlantic, characterizing LSf25 in many ways as a classical hosing experiment, where a deep-water formation region is forced with an anomalous freshwater flux.

BSf25, on the other hand, aims at amplifying already occurring transports of sea ice and freshwater, such as the transport through Denmark Strait. In the CTRL, roughly 5200 $\mathrm{km^3\,yr^{-1}}$ of freshwater flow southward through the Denmark Strait in solid and liquid form (applying a reference salinity of 34.7; for calculation of

freshwater transport, see, e.g., Lehner et al. 2012b). In the transient simulations this transport increases from MCA to LIA by about 400 $km^3 yr^{-1}$, primarily driven by larger sea ice transport. In BSf25 approximately 2800 $km^3 yr^{-1}$ of freshwater is added as artificially grown sea ice in the Barents Sea. However, the Denmark Strait transport increases only by about 1000 $km^3 yr^{-1}$. Thus, about two-thirds of this additional freshwater stays north of Denmark Strait, for example, as on average about 1.5-m-thicker sea ice in the Arctic. A large portion of this 1000 $km^3 yr^{-1}$ is made up by liquid freshwater. This indicates that part of the additional sea ice from the Barents Sea melts on its way to Denmark Strait. The sea ice portion of this increased Denmark Strait transport (about 100 $km^3 yr^{-1}$) is nonetheless crucial for the experimental purpose of mimicking the MCA–LIA changes as sea ice is more potent in disturbing convection sites than advection of liquid freshwater (Born et al. 2010).

Clearly, these imbalances are not optimal: however, the comparison reveals them to be of moderate magnitude. More importantly, it is shown that the sensitivity experiments simulate the processes as intended, that is, a direct disturbance of the convective site in the Labrador Sea (in LSf25) and an increased transport of sea ice and freshwater through Denmark Strait (in BSf25). Additional comparisons with the transient simulations further strengthen the confidence in the design of the sensitivity experiments (see section 4).

3. Transition from the Medieval Climate Anomaly to the Little Ice Age

The simulations with transient forcings aim at realistically simulating the transition from the MCA to the LIA. By using a six-member ensemble of these transient simulations we are able to obtain robust results that stand out against the natural variability inherent in the sixfold simulation of this specific time period (6 × 351 yr). In the following, we first present the significant changes during the transition phase, which occur because of the negative forcing. Additionally, we identify a positive sea ice–ocean feedback mechanism in these simulations that substantially amplifies these changes and is potentially able to sustain the cold conditions of the LIA even in the absence of negative forcing. Based on the results of our transient ensemble simulations we summarize this feedback hypothesis, containing two feedback loops (in what follows we use the term ''feedback mechanism'' to describe collectively both feedback loops). In the subsequent section we then test the hypothesis in the framework of artificial sea ice growth experiments.

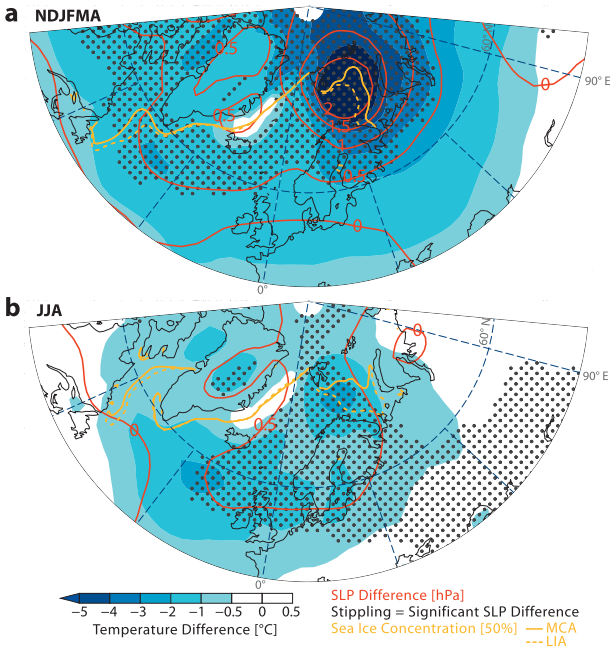

FIG. 4. Little Ice Age minus Medieval Climate Anomaly [LIA (1450–1500) − MCA (1150–1200)] difference in sea level pressure, surface air temperature (only significant differences are colored), and sea ice concentration for (a) November–April means and (b) for June–August means. Significance at the 5% level is tested with a two-sided *t* test.

a. Main climate response

Shortly after initialization of the transient simulations the Northern Hemisphere temperature starts to decrease in response to the decreasing total solar irradiance and the large volcanic eruptions occurring between 1150 and 1300 AD (Fig. 2c). In particular, the large eruption in 1258 AD and the three smaller ones following shortly after cause a significant hemispheric cooling. After about a century of stable TSI and few volcanic eruptions between 1300 and 1400 AD, the Spörer Minimum with its pronounced TSI minimum and two large eruptions in the 1450s cause another temperature drop, coinciding with the beginning of the coolest period of the last millennium in reconstructions (~1400–1700 AD, e.g., Mann et al. 2009).

As another consequence of the negative forcing at the beginning of the transition period, sea ice extent and volume increase in the entire Arctic region. In the transient simulations, the largest expansion of sea ice occurs in the Atlantic sector, namely, the Barents and Labrador Seas (Fig. 4). In the Barents Sea, the enhanced sea ice cover reduces the strong ocean–atmosphere heat flux from the warm Atlantic waters that usually enter the Barents Sea. As this local heat source weakens, a significant elevation of SLP over the Barents Sea develops (Hoskins and Karoly 1981) and becomes the dominant

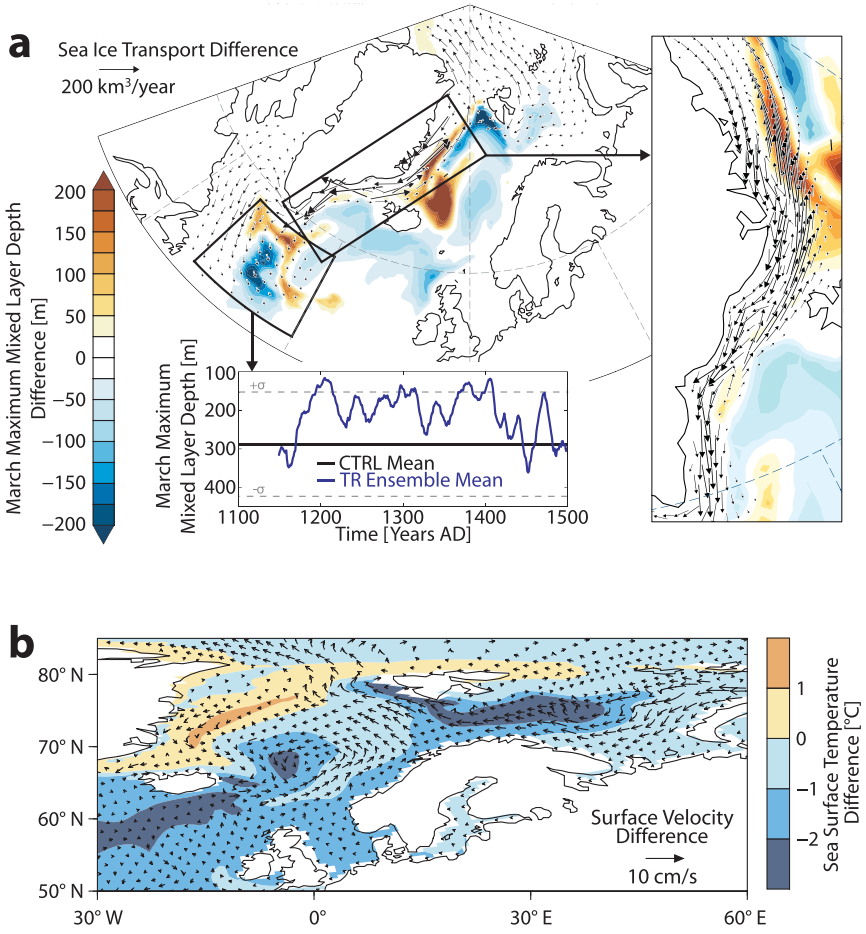

FIG. 5. (a) LIA − MCA difference in sea ice transport (November–April means, only differences >15 $km^3\,yr^{-1}$ are shown) and LIA − MCA March maximum mixed layer depth (time series is ensemble mean 5-yr running mean averaged over indicated region). The inset zooms in on the anomalous southward transport of sea ice along the coast of Greenland. (b) LIA − MCA difference in annual mean ocean surface currents (top 15 m) and sea surface temperature.

feature of winter atmospheric circulation change during that time (Fig. 4a). This SLP anomaly does not translate into a strong high pressure system as in, for example, Petoukhov and Semenov (2010), but into a horizontal contraction of the northern center of action of the NAO. The direct thermal effect of the capped ocean–atmosphere heat flux together with increased advection of cold Arctic air due to the SLP anomaly cause enhanced cooling over the Barents Sea and Northern Europe, both in winter and—to a lesser degree—in summer (Figs. 4a,b).

b. Feedback mechanism

1) ARCTIC–NORTH ATLANTIC FEEDBACK LOOP

The first feedback loop starts with an increase of sea ice in the Barents Sea, a region known to be a strong source of sea ice, where a large part of the sea ice produced locally is exported to the Arctic Ocean. The Arctic Ocean itself exports sea ice mainly through Fram Strait (~97% in CTRL), where indeed the annual sea ice transport is slightly increased (from 3280 to 3450 $km^3\,yr^{-1}$). A portion of the Barents Sea sea ice is also exported to the Nordic Seas by the exiting branch of the East Spitsbergen Current, which strongly increases its transport of sea ice (from 100 to 310 $km^3\,yr^{-1}$) from the MCA to the LIA. While part of the anomalous sea ice being exported from the Barents Sea and the Arctic Ocean melts in the Nordic Seas, another part is transported farther south by the East Greenland Current, eventually being carried around the southern tip of Greenland to reach the Labrador Sea (Fig. 5a). Finally, the sea ice melts either in the Labrador Sea or in the adjacent subpolar North Atlantic. With the decreasing radiative forcing at the inception of the LIA, the portion that melts in the Labrador Sea gets smaller

while the portion exported to the North Atlantic grows (not shown). Changes in sea ice volume transport through Denmark Strait are dominated by changes in sea ice volume rather than circulation. Therefore, transport anomalies pointing northward indicate reduced ice thickness rather than reversed transport direction (Fig. 5a).

In the North Atlantic the melting sea ice then causes a temperature and salinity drop at the sea surface, which leads to increased stratification and weakened convection, illustrated by a shoaling of the mixed layer depth at the Labrador Sea exit (Fig. 5a). Thereby the surface waters become lighter and decrease the sea surface height (SSH) gradient that drives the subpolar gyre (SPG). The SPG (average of barotropic streamfunction within 48°–65°N, 60°–10°W) weakens by 5% from the MCA to the LIA, closely followed by a 7% weakening of the AMOC (maximum of the meridional overturning circulation in the Atlantic north of 28°N). A 2-yr lag correlation between the two indices of 0.75 ($p < 0.001$, based on annual means) illustrates the near-synchronous basinwide circulation slowdown. Consequently, the heat and salt transport into the Nordic Seas, the Barents Sea, and the Arctic Ocean decreases as well (not shown). This causes the mixed layer depth to shoal in the northern Nordic Seas as well (Fig. 5a), which in turn weakens the overturning cell in the Nordic Seas (not shown). As the sea ice in the central Arctic Ocean thickens, initial sea ice growth and the accompanied brine rejection are decreased, which leads to a weakening of the convection also in the Arctic Ocean (similar to Zhong et al. 2011). This ultimately results in a reduced northward heat transport that, in turn, reinforces sea ice growth in the Barents Sea and thereby closes the positive feedback loop.

2) BARENTS SEA FEEDBACK LOOP

Our simulations indicate that in addition to the overall reduced heat transport into the Nordic Seas there is a more regional feedback loop, which involves the reorganization of ocean currents in the Nordic Seas. The Norwegian Atlantic Current usually carries warm and salty Atlantic waters up to the Barents Sea opening where it is partitioned into Barents Sea inflow, West Spitsbergen Current, and waters recirculating in the Nordic Seas. During the MCA–LIA transition, the recirculating current strengthens and redirects the warm Atlantic waters toward Greenland, resulting in elevated sea surface and air temperatures east of Greenland (Figs. 4 and 5b). At the same time the other currents transport less water. The Barents Sea inflow (calculated as the difference of the barotropic streamfunction between Spitsbergen and the North Cape), for example, is reduced by 35%, corresponding to 1.27 Sv (Fig. 6a). As

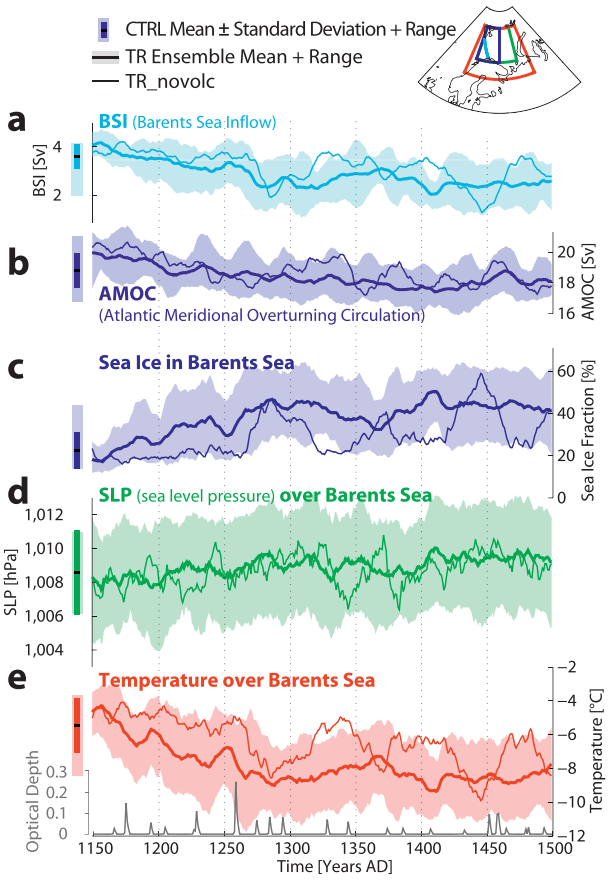

FIG. 6. (a) Barents Sea inflow as difference of barotropic streamfunction between Spitsbergen and Norway (see map) and Atlantic meridional overturning circulation as maximum of the meridional overturning circulation north of 28°N. (b) Sea ice concentration in the western Barents Sea (see map). (c) Sea level pressure and (d) temperature over the Barents Sea (see map) and annual-mean optical depth changes due to volcanic eruptions. All time series, except optical depth, are 5-yr running means from annual means. Long-term annual mean, ±1 standard deviation of annual means, and range of 5-yr running means from CTRL are indicated as bars on the left side. Colors in time series correspond to the colored areas outlined in the map.

a consequence of the reduced inflow of warm waters, the sea ice edge in the Barents Sea advances farther south (Fig. 6c), leading in turn to increased SLP (Fig. 6d) and a strong drop in regional temperature (Fig. 6e).

To further investigate the mechanisms causing the decreased Barents Sea inflow, we select a transect across the Barents Sea opening (Fig. 7). The LIA–MCA difference in ocean density indicates that the Barents Sea shelf becomes lighter as we move toward the LIA (Fig. 7c). This can be attributed to the increased sea ice cover as well as to the reduced inflow of salty Atlantic waters, both contributing to surface freshening that reduces density. Indeed, the density differences in the Barents Sea are largest at the surface, thereby strengthening the

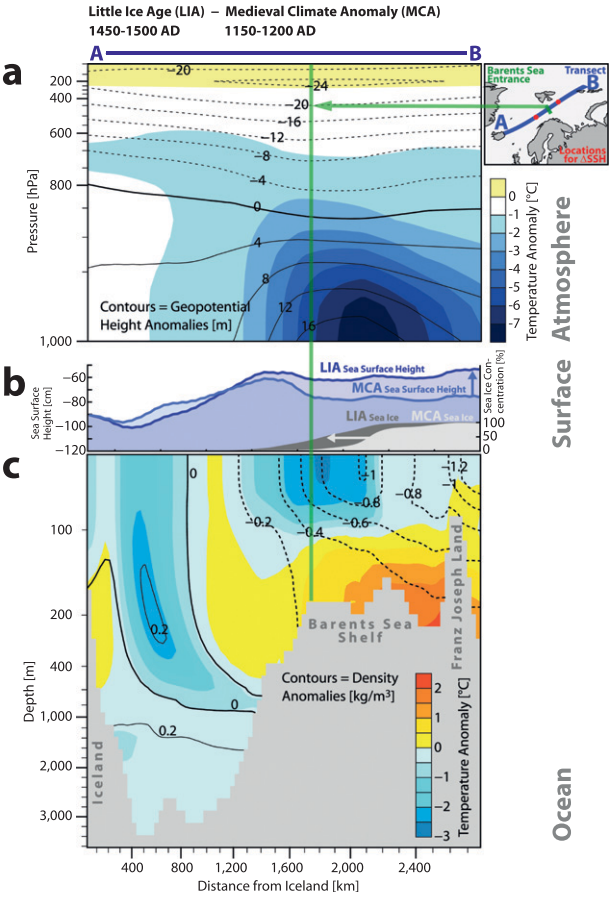

FIG. 7. Transect across the Barents Sea from Iceland (A, see map) to Franz Josef Land (B). LIA − MCA winter (November–April) difference in (a) air temperature and geopotential height, (b) sea surface height (as anomaly from global mean, which is zero) and sea ice concentration, and (c) ocean density (contours) and temperature (shading). The red dots on the map indicate the locations used to derive SSH-driven transport anomalies across the Barents Sea opening (see text for details).

halocline. The strong halocline in turn forces the warm and salty Atlantic waters that enter the Barents Sea to subside below the lighter surface waters, causing a warming below approximately 100 m (Fig. 7c) and reinforcing the freshening of the upper 100 m. The Nordic Seas, on the other hand, become denser owing to the recirculating Atlantic waters (Fig. 7c). These opposing density trends result in a stronger SSH gradient across the Barents Sea transect (Fig. 7b), which will drive an anomalous circulation (see below).

The LIA–MCA differences in the sea ice concentration (Fig. 7b), SLP (expressed as geopotential height), and air temperature (Fig. 7a) in the Barents Sea transect indicate a strong ocean–atmosphere coupling: the largest atmospheric cooling occurs exactly over the advanced sea ice edge, caused by the covered ocean surface heat flux. The near-surface cooling, in turn, causes air to descend and geopotential height and SLP to increase over the Barents Sea. This local baroclinic response is consistent with atmosphere-only sensitivity experiments by Petoukhov and Semenov (2010), in which sea ice concentration in the Barents–Kara Sea region was prescribed to change from 80% to 100% (similar to the MCA–LIA changes from 88.5% to 96.7% over the same region in our transient simulations). However, for sea ice concentration changes from 80% to 40% Petoukhov and Semenov found a barotropic response, indicating possible nonlinearities in the sea ice–atmosphere coupling. The increased SLP over the Barents Sea implies changes in wind stress and Ekman transport. Such changes have been discussed as potential causes for changes in ocean circulation, such as a strengthened recirculation in the Nordic Seas or a reduction of the Barents Sea inflow (Semenov et al. 2009). In our study, the annual mean Ekman transport integrated over the Barents Sea opening (0.33 ± 0.38 Sv in CTRL) is an order of magnitude smaller than the actual total Barents Sea inflow (3.58 ± 0.79 Sv in CTRL), in good agreement with observational estimates of this relation (Ingvaldsen et al. 2004). Further, the Ekman transport integrated over the Barents Sea opening does not change significantly from the MCA to the LIA (+0.06 Sv), while the total Barents Sea inflow decreases by 1.27 Sv, thereby outruling Ekman transport as the direct driver of the reduced Barents Sea inflow during the LIA.

Instead, the reduction of the Barents Sea inflow from the MCA to the LIA can be explained by the SSH gradient change of 0.146 m across the Barents Sea opening (see Fig. 7 for the location of the two points used to calculate the SSH gradient). The change in the Nordic Seas recirculation is estimated by applying the geostrophic equation together with the distance across δx (940×10^3 m) and depth z (183 m) of the Barents Sea opening:

$$\Delta F_g = -\frac{g}{f}\frac{\Delta\delta\eta}{\delta x} z \delta x, \qquad (2)$$

where ΔF_g is the change in geostrophic volume transport, g the gravitational acceleration, f the Coriolis parameter at 75°N, and $\Delta\delta\eta$ is the change in the SSH gradient. Using the LIA–MCA change in $\delta\eta$ of 0.146 m, ΔF_g amounts to −1.86 Sv, indicating a substantial strengthening of the recirculation. The SSH-driven changes of the Norwegian Coastal Current, on the other hand, are an order of magnitude smaller (not shown). Considering continuity in the partitioning of the water masses in the Nordic Seas, this implies that the reduction of the Barents Sea inflow of −1.27 Sv is largely a consequence of the

strengthened recirculation in the Nordic Seas. The SSH anomalies in the Barents Sea are primarily density driven, however, changes in Ekman transport within the Barents Sea contribute as well: density anomalies at the location used to calculate the SSH gradient (see map in Fig. 7) explain 64% of the SSH gradient change, leaving the remaining 36% to wind-induced rearrangement of the water masses within the Barents Sea. It therefore appears that, in summary, the initial sea ice growth in the Barents Sea reinforces itself via sustained weakening of the Barents Sea inflow, which in turn is caused by sea ice–induced changes in both density and winds over the Barents Sea.

c. *Excluding volcanic eruptions*

One additional transient simulation was conducted, from 1150–1500 AD, in which volcanic eruptions were excluded (TR_novolc). Figure 2c shows that in TR_novolc the Northern Hemisphere cools with a comparable magnitude as in the transient simulations including volcanic eruptions, which might raise the question whether volcanic eruptions are at all needed to explain the inception of the LIA. However, the applied solar forcing has a relatively large amplitude and, therefore, likely dominates the cooling trend in both the transient ensemble simulations and in TR_novolc. Given the still open discussion on past TSI amplitudes, this prevents us from concluding that volcanic forcing is a noncrucial factor for triggering the LIA. Further, Zhong et al. (2011) have shown that, when starting from slightly colder conditions (their control simulation applies a $1.4\,\mathrm{W\,m^{-2}}$ weaker TSI than this study's CTRL), volcanic forcing alone can lead to significant hemispheric cooling and consequent sea ice expansion.

Additional evidence for the importance of volcanic forcing comes from Fig. 2d, where the lack of volcanic eruptions causes a larger discrepancy between the transient ensemble and TR_novolc than in case of the Northern Hemisphere temperature (Fig. 2c). Also, Figs. 6c,e show that in the Barents Sea the absence of volcanic eruptions results in only intermittent periods of increased sea ice fraction and decreased temperatures. In particular, this is evident during the period 1150–1250 AD, when TSI is roughly unchanged compared to CTRL and the largest forcing impact would come from volcanic eruptions. However, over the full length of the simulation all quantities stay within the range of the transient ensemble, qualitatively reproducing the MCA–LIA transition (Fig. 6). Thus, sequenced volcanic eruptions appear to be crucial for maintaining an expanded sea ice margin, but not for triggering the overall climate response.

4. Artificial sea ice growth experiments

The sensitivity experiments, BSf25 and LSf25, aim at simulating specific aspects of the sea ice changes occurring during the MCA–LIA transition and thereby try to determine the role of the Barents and Labrador Seas in this transition. In both sensitivity experiments artificial sea ice growth occurs during the first 100 years. During the second 100 years, this forcing is switched off to observe how fast the system returns to its initial state. We first discuss the results of the experiments in context of the MCA–LIA climate transition. In a second part, additional technical details about the experiments are presented.

a. *Main climate response*

The anomalies in SLP, temperature, and sea ice from years 50–99 of LSf25 and BSf25 against the CTRL (Figs. 8a,b) bear strong resemblance with the LIA–MCA anomalies from the transient simulations (Fig. 4a): an advanced sea ice edge in the Barents Sea geographically coincides with increased SLP and decreased temperatures. At the same time the western Nordic Seas experience a warming owing to a strengthened recirculation (Figs. 8c,d). Thus, the sensitivity experiments show that a climate response qualitatively similar to the transient simulations can be induced by the artificial sea ice growth in either of the two regions, Barents or Labrador Seas.

b. *Feedback mechanism*

We investigate the same indices as in the transient simulations to identify the Arctic–North Atlantic feedback loop as well as the more regional Barents Sea feedback loop in the sensitivity experiments (Fig. 9).

In the BSf25 experiment, the sea ice concentration in the Barents Sea increases rapidly as the artificial sea ice growth starts (Fig. 9b). At the same time, the Barents Sea inflow is weakened by about 50%, overlaid by natural variability such as a short-lived resumption after about 40 yr (Fig. 9a). Not surprisingly, this short-lived resumption—with a small lag—can be identified in the sea ice index, illustrating the sensitivity of the Barents Sea sea ice cover to the inflow of warm Atlantic waters. The AMOC, on the other hand, remains in the range of natural variability until around model year 45, when it drops below the 1-σ range of CTRL (Fig. 9b). This time lag resembles the chain of events from excess sea ice production in the Barents Sea, the transport of this sea ice through Fram Strait and along the east side of Greenland, its engagement in the convective feedback in the Labrador Sea, and ultimately the substantial weakening of the AMOC. In accordance with the

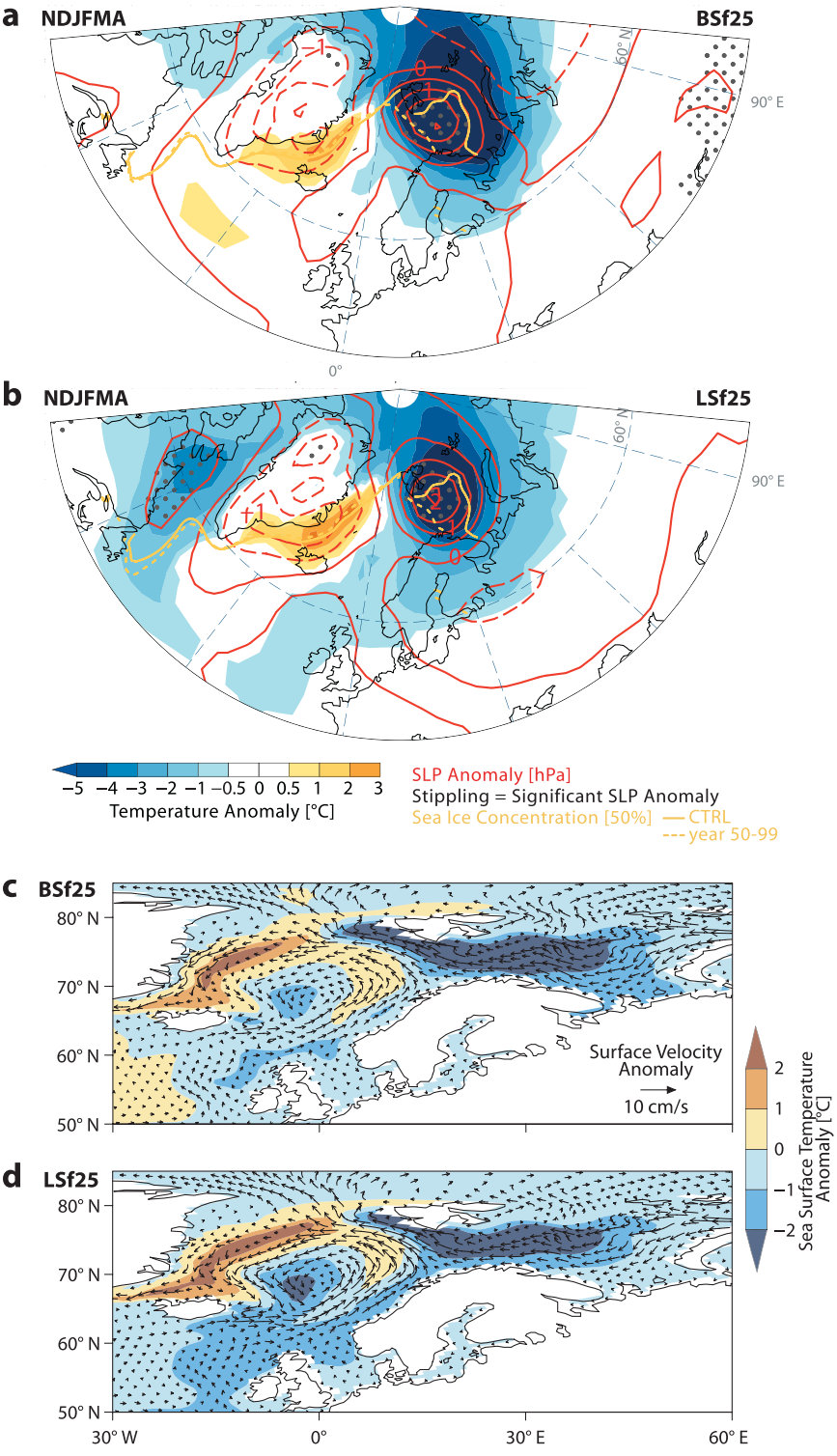

FIG. 8. (a),(b) Anomalies in sea level pressure, surface air temperature (only significant anomalies are colored), and sea ice concentration for November–April means from the years 50–99 of (a) BSf25 (artificial sea ice growth in Barents Sea) and (b) LSf25 (artificial sea ice growth in Labrador Sea) − mean of CTRL. Significance of SLP changes is tested at the 5% level with a two-sided *t* test. (c),(d) Anomalies of annual mean ocean surface currents (top 15 m) and sea surface temperature from the years 50–99 of (c) BSf25 − mean of CTRL and (d) LSf25 − mean of CTRL.

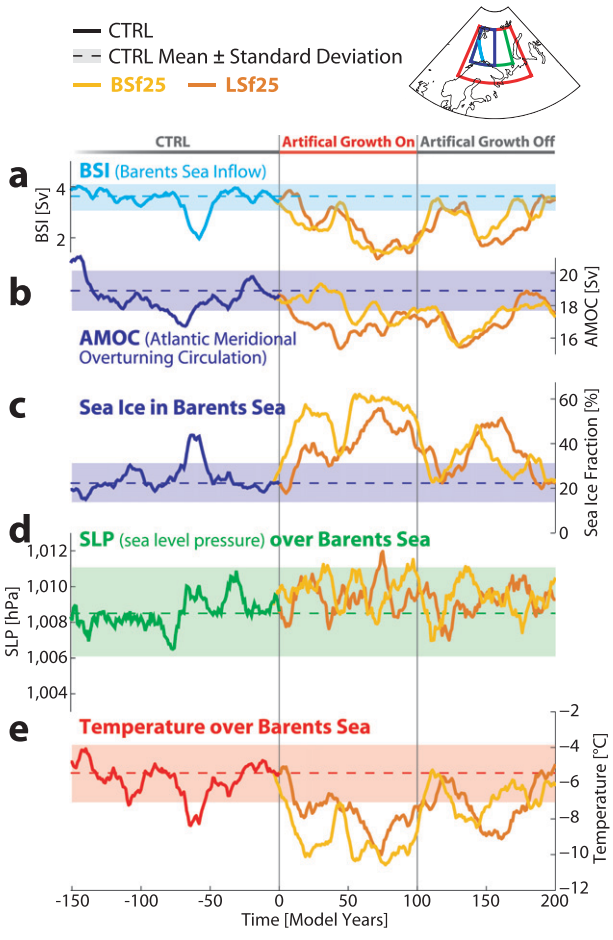

FIG. 9. As in Fig. 6 but for CTRL (only 150 yr are shown), BSf25, and LSf25. All time series are 5-yr running means; however, the standard deviation is based on annual values of the entire CTRL 494 yr. Colors in time series for t < 0 correspond to the colored areas outlined in the map.

advancing sea ice edge in the Barents Sea, regional SLP and temperature rise and fall, respectively (Figs. 9d,e). This shows that in the BSf25 experiment the interplay between Barents Sea sea ice cover, Barents Sea inflow, SLP, and temperature is at work decades before the AMOC responds and itself influences the Nordic Seas. Therewith the independence and full closure of the Barents Sea feedback loop is illustrated.

In LSf25 the artificial sea ice growth transforms the Labrador Sea into a strong sea ice source. The additional sea ice is melted in situ or exported to the adjacent subpolar North Atlantic (not shown). In any case, the strong freshwater forcing from the additional sea ice reduces convection in the North Atlantic and leads to a constant reduction of the AMOC until about model year 50, when it stabilizes (Fig. 9b). With a lag of about 10 yr, the Barents Sea inflow starts to weaken as well, a relation which matches our observations from CTRL, where the AMOC leads the Barents Sea inflow on average by 13 yr ($r = 0.66$, $p < 0.01$ on 5-yr running means). Further, this lag of about one decade is reminiscent of the time scale associated with advection of salinity anomalies in the SPG, as they have been observed (e.g., Dickson et al. 1988; Belkin 2004) and modeled (e.g., Häkkinen 1999) in context of the great salinity anomalies of the twentieth century. As soon as the inflow of Atlantic water weakens, the sea ice in the Barents Sea starts to increase, thereby, again, mirroring variability of the inflow. As a consequence of the increased sea ice cover in the Barents Sea, SLP rises and temperature falls (Figs. 9d,e). From this point on, the two sensitivity experiments qualitatively agree, illustrating the connection of the two regions, the Barents and Labrador Seas, via a complex feedback mechanism.

There is evidence from CTRL that this feedback mechanism is active already in the control climate, however, in the absence of negative external forcing is unable to destabilize the system in a sustainable manner. Figure 9 shows that, in the 150 yr of CTRL leading up to the start of the sensitivity experiments, there occurs a short excursion of all quantities that very much resembles the feedback mechanism: the AMOC falls below the 1-σ range of the CTRL at about −60 yr, upon which the Barents Sea inflow drops markedly, sea ice and SLP increase, and temperature falls (Figs. 9a–e). However, all quantities return to CTRL mean values within 10–15 yr as the circulation changes are not large enough as to qualitatively change the discussed feedback mechanism.

c. *Self-sustained feedback mechanism*

The existence of apparently destabilizing positive feedback loops raises the question of self-sustainability of such feedback loops. Zhong et al. (2011) found the Arctic–North Atlantic feedback loop to be self-sustaining in two out four cases, whereby they revealed necessary preconditions for the North Atlantic. To test whether this self-sustainability exists in our experiments as well, we stop the artificial sea ice growth after 100 yr. In both sensitivity experiments the Barents Sea sea ice edge retracts to CTRL levels within a decade (Fig. 9c). This is primarily a result of sea ice top melt, which is large owing to the perpetual high solar irradiance in 1150 AD. In the absence of the artificial sea ice growth, this process acts to quickly push back the sea ice edge. As the sea ice retreats, the SSH gradient across the Barents Sea opening weakens, and the Barents Sea inflow recovers (Fig. 9a). It therefore seems that the smaller-scale Barents Sea feedback loop is not self-sustaining. The AMOC, however, remains on a reduced level for decades, eventually triggering another passage of the Arctic–North

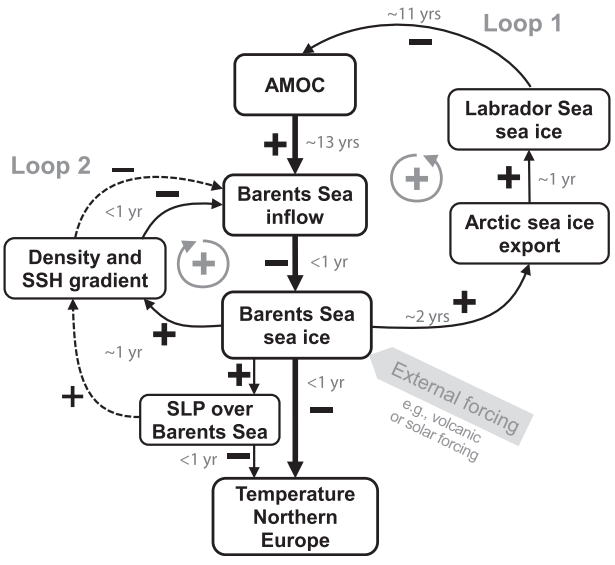

FIG. 10. Schematic overview of the feedback loops associated with the Medieval Climate Anomaly–Little Ice Age transition, including estimates of time lags. Positive correlation between two processes is indicated with a plus sign, negative correlation with a minus sign. Negative external forcing leads to increased sea ice in the Arctic, especially in the Barents Sea. Loop 1: this causes an increased Arctic sea ice export and subsequently an increased import of sea ice into the Labrador Sea. As this sea ice melts, it weakens the Atlantic meridional overturning circulation, which in turn reduces the Barents Sea inflow of warm waters, causing further sea ice growth. Loop 2: increased sea ice causes the Barents Sea to become fresher and less dense. Additional but slightly less important wind changes due to elevated sea level pressure increase the sea surface height in the Barents Sea (dashed). As a result of these two processes, the SSH gradient across the Barents Sea opening increases, further reducing the Barents Sea inflow and thereby supporting sea ice growth. Finally, the increased sea ice cover has a direct thermal effect, decreasing surface air temperatures over Northern Europe and an indirect effect by inducing elevated SLP that allows for the advection of cold Arctic air toward Europe.

Atlantic feedback loop, thereby also triggering the Barents Sea feedback loop again: about 40 yr after switching off the artificial sea ice growth the Barents Sea inflow weakens (Fig. 9a), leading to increased sea ice (Fig. 9c), elevated SLP (Fig. 9d), and cooler temperatures (Fig. 9e). The two experiments conducted here provide evidence that the European climate is vulnerable to destabilizing positive feedbacks, given the appropriate external trigger in the form of negative radiative forcing. The sustained weakening of the AMOC is able to move the North Atlantic–European climate to a cooler state and keep it there for decades. Figure 10 summarizes the feedback mechanism and depicts the two feedback loops at work.

Figure 11 depicts the changes occurring in sea ice volume and sea ice volume tendency as a response to the artificial sea ice growth. On a hemispheric scale the sea ice volume increase over the first 100 yr in BSf25 and LSf25 ($+13.3 \times 10^3\,km^3$ and $+13.4 \times 10^3\,km^3$, respectively) is of a similar magnitude as the one found in the transient simulations from MCA to LIA ($+15.7 \times 10^3\,km^3$; Fig. 11a). This also implies that the sea ice growth rate (given as thermodynamic volume tendency) in BSf25 and LSf25 is significantly larger than in the transient simulations, as there the sea ice volume increase takes place over a longer time period (351 yr instead of only 100 yr). After stopping the artificial sea ice growth in both experiments BSf25 and LSf25 the hemispheric sea ice volume remains elevated compared to CTRL, confirming the self-sustainability of the feedback mechanism discussed before.

The Barents Sea during CTRL is in near balance regarding annual-mean sea ice production and export (Fig. 11b). Until the LIA, however, the Barents Sea has become a net source of sea ice in the transient simulations. Nonetheless, the Barents Sea's own sea ice volume has also increased. This behavior is successfully mimicked in the BSf25 experiment, as sea ice growth and export, as well as sea ice volume, strongly increase during the first 100 yr. During the second 100 yr, the sea ice volume is reduced again, but the Barents Sea retains its role as a sea ice source. Interestingly, the same behavior is observed when we artificially grow sea ice in the Labrador Sea (LSf25), which illustrates the inherent linkage of the Labrador and Barents Seas that constitutes our feedback mechanism: that is, the linkage of the two feedback loops.

In contrast to the Barents Sea, the Labrador Sea is a sea ice sink (in CTRL, but also during the MCA–LIA transition; Fig. 11c). At the inception of the LIA, both import and melting of sea ice increase, which is in line with the shoaling of the mixed layer depth in the region of the Labrador Sea (Fig. 5a). During the LSf25 experiment, however, sea ice grows in the Labrador Sea and is then exported to the subpolar North Atlantic, leading to a reduction in the AMOC similar to the transient simulations. Once the artificial sea ice growth is stopped, the Labrador Sea switches back into the role of a sea ice sink, and the sea ice volume decreases rapidly. During the BSf25 experiment, the Labrador Sea imports more sea ice, and melting is increased as well, compared to CTRL. Thereby, the behavior of the Labrador Sea during the MCA–LIA transition is mimicked, and the linkage of the Labrador and Barents Seas is illustrated again, this time in the opposite direction.

5. Discussion and conclusions

This study investigates the role of sea ice–ocean–atmosphere coupling in shaping regional climate during

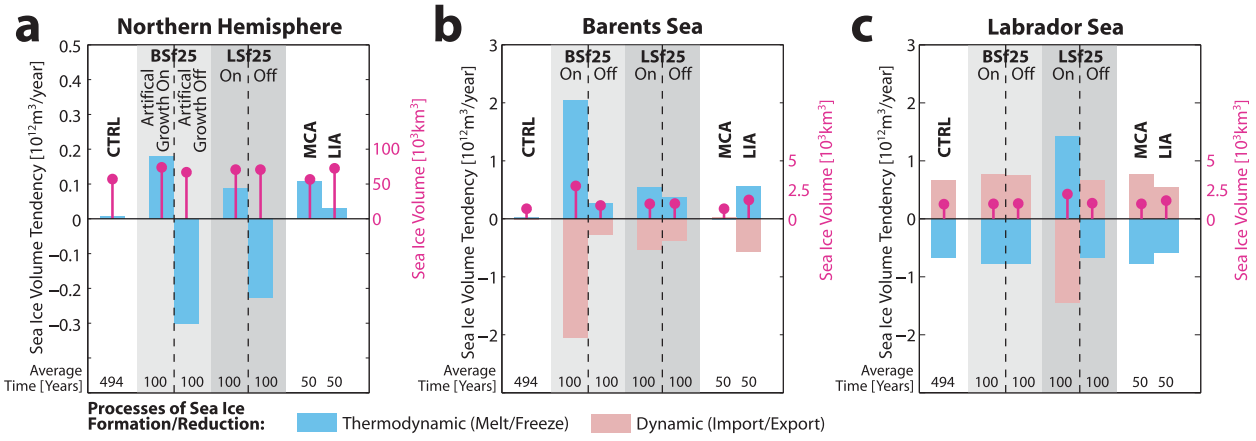

FIG. 11. Annual mean sea ice volume tendency (split up in thermodynamic and dynamic terms; blue and red bars, left *y* axis) and sea ice volume (thin magenta bars with dots, right *y* axis) integrated over (a) the Northern Hemisphere from CTRL, from the artificial sea ice growth experiments (BSf25 and LSf25, grouped in two 100-yr intervals during which artificial sea ice growth was switched on and off, respectively), and from the transient simulations (Medieval Climate Anomaly: 1150–1200 AD, Little Ice Age: 1450–1500 AD). (b),(c) As in (a) but for (b) the Barents Sea and (c) the Labrador Sea.

the inception of the Little Ice Age. Using an ensemble of transient simulations with CCSM3 we find the transitional phase from MCA to LIA to be dominated by a cooling and strong advances in sea ice cover on the Northern Hemisphere. In the Barents Sea, the advancing sea ice cover reduces the ocean–atmosphere heat flux and thereby cools the larger area. Additionally, increasing SLP over the Barents Sea allows for southward advection of cold Arctic air, resulting in an enhanced cooling over Northern Europe that qualitatively fits well with proxy-based temperature reconstructions (Mann et al. 2009). This chain of events offers an explanation for the regional temperature evolution during the MCA–LIA transition that does not rely on significant changes in the NAO, which are ambiguous (Trouet et al. 2012) and are not found to occur in several simulations using state-of-the-art coupled atmosphere–ocean climate models (Lehner et al. 2012a; Yiou et al. 2012). There remain, however, questions on the role of the stratosphere–troposphere coupling in the context of low-frequency variability of the atmosphere and the ability of climate models to simulate this coupling (e.g., Spangehl et al. 2010; Manzini et al. 2012). The majority of the climate models (including CCSM3) of phase 3 of the Coupled Model Intercomparison Project (CMIP3) apply only relatively crude stratospheric dynamics, owing to low vertical resolution of the stratosphere (e.g., Cordero and Forster 2006). This has been suggested as cause for them not reproducing the low-frequency atmospheric variability proposed by the reconstruction (e.g., Mann et al. 2009).

Confirming and expanding findings by Zhong et al. (2011), we identify a sea ice–ocean feedback loop that lays the foundation for the changes in surface climate described above. Following negative radiative forcing from volcanic eruptions and decreasing total solar irradiance at the inception of the LIA (1150–1300 AD), Arctic sea ice volume and extent grow significantly. As this anomalous sea ice is increasingly exported to the Labrador Sea and subpolar North Atlantic, it cools and freshens the surface waters and reduces convection. Consequently, the subpolar gyre and the AMOC are weakened, which leads to reduced transport of heat into the Nordic Seas, the Barents Sea, and the Arctic Ocean. Weakening of convective deep-water formation in the Nordic Seas and the Arctic Ocean further reduces the import of heat, thereby reinforcing the initial sea ice expansion.

In addition, another feedback loop between the Barents Sea and the Nordic Seas further amplifies the sea ice growth and regional cooling at the beginning of the LIA. Upper-ocean density changes, together with wind-driven reorganization of water masses, increase the Barents Sea SSH, ultimately reducing the inflow of warm Atlantic waters into the Barents Sea and strengthening the recirculation in the Nordic Seas. Contrary to Semenov et al. (2009), changes in Ekman transport at the Barents Sea opening are found to be negligible. Using sensitivity experiments with artificial sea ice growth in the Barents and Labrador Seas, we are able to prove the existence and closure of both feedback loops detected in the transient simulations. After switching off the artificial sea ice growth for the second 100 years of the experiments, Arctic sea ice remains in an expanded state for decades, confirming the potential self-sustainability of the Arctic sea ice cover attributed to these feedback loops (Zhong et al. 2011).

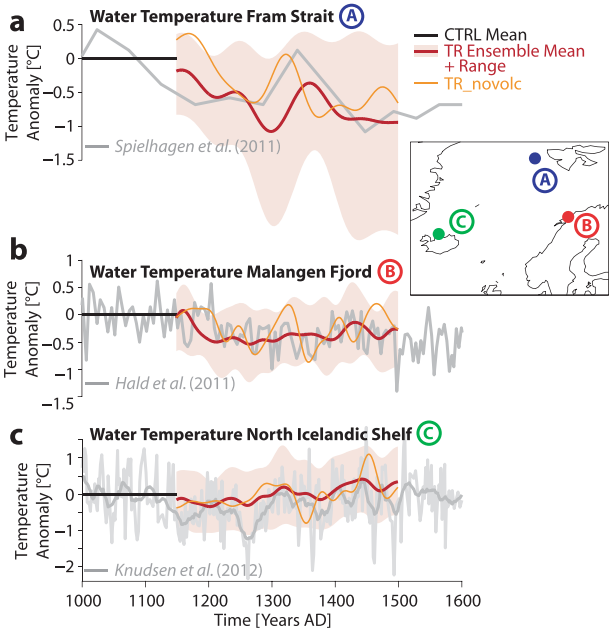

FIG. 12. (a) Water temperature anomaly in the eastern Fram Strait from Spielhagen et al. (2011) (wrt 823–1074 AD) and in the model simulations (wrt long-term mean of CTRL; ~78°N, 8.5°–11.5°E; average over 200–300-m depth). (b) Water temperature anomaly in the Malangen Fjord from Hald et al. (2011) (wrt 1000–1149 AD) and in the model simulations (40-yr Fourier filtered; wrt long-term mean of CTRL; ~70°N, 16.5°–18.1°E; at 47-m depth). (c) Water temperature anomaly (annual and 5-yr running mean; wrt 1001–1150 AD) on the north Icelandic shelf from Knudsen et al. (2012) and in the model simulations (40-yr Fourier filtered; wrt long-term mean of CTRL; ~66.0°–67.0°N, 19.0°–21.3°E; at surface).

Support for this modeling result comes from new foraminifera-based proxies in Fram Strait (Spielhagen et al. 2011) and off the coast of a Norwegian fjord (Hald et al. 2011). Water temperatures in both proxies are controlled largely by the amount of Atlantic waters in the mean flow as the proxies are located on distinct pathways for Atlantic waters into the Arctic. At these locations a near-synchronous drop in upper-ocean water temperature occurred at the onset of the LIA, indicating a reduced amount of Atlantic waters arriving (Figs. 12a,b). This shift is remarkably well reproduced by the model, which captures both the timing and magnitude of the shift. Further, new results from the north Icelandic shelf indicate a small temperature increase during the MCA–LIA transition (Fig. 12c, Knudsen et al. 2012) that corresponds to a northward shift of the oceanic polar front, allowing Atlantic species to enter the Nordic Seas. This signal is reproduced as well by the model, corroborating the coherent picture of oceanic changes in the Nordic Seas during the MCA–LIA transition: while the overall heat transport into the Nordic Seas is reduced, changes in the distribution of the Atlantic water leave a distinct pattern of localized warming and cooling around the Nordic Seas.

Excluding volcanic eruptions in one of the transient simulations yields a similar hemispheric temperature and sea ice response as in the simulations with volcanoes; however, the sea ice cover does not consequently remain in its expanded state as compared to the all-forcing simulations (both Arctic-wide and in the Barents Sea). Nevertheless, it appears that the origin of the negative forcing (TSI or volcanoes) is not crucial as long as it is persistent enough to trigger the destabilizing feedback mechanism described in this study. As the amplitude of the past TSI variations and therewith its importance in triggering the MCA–LIA transition remains debated (e.g., Gray et al. 2010; Shapiro et al. 2011; Miller et al. 2012), it is difficult to attribute quantitative importance to either of the two forcings. While this is a pressing question in the context of paleoclimate sensitivity, it is beyond the scope of this study.

Further, many recent studies describe large events of internal variability in the climate system that are able to derail temperature and sea ice from the path anticipated solely from the external forcing: Kinnard et al. (2011) suggest that Arctic summer sea ice decreased post-1500 AD (i.e., during a period of negative forcing), a suggestion for which Crespin et al. (2009) provide support from modeling with data assimilation. However, both studies acknowledge that the absence of changes in heat transport into the Arctic Ocean during that time (Spielhagen et al. 2011) complicates the explanation for such anomalous behavior in Arctic temperature and sea ice.

Along the same lines, nonlinear dynamics such as the feedbacks described in this study can depend crucially on the background climate, as shown also at the example of climate impacts of volcanic eruptions (e.g., Otterå et al. 2010; Zhong et al. 2011; Zanchettin et al. 2012) or ocean–atmosphere coupling (e.g., Yoshimori et al. 2010). To that end, transient ensemble simulations as well as sensitivity experiments, together with new proxies, will help to constrain the uncertainties associated with the MCA–LIA transition and improve our understanding of mechanisms governing climate on the regional scale.

Acknowledgments. We gratefully acknowledge David Bailey, Marika Holland, Alexandra Jahn, Dirk Notz, and Bette Otto-Bliesner for valuable discussions; Katrine Husum, Karen Luise Knudsen, and Alexander Shapiro for providing proxy data; and two anonymous reviewers for constructive comments. We are grateful to the NCAR in Boulder, Colorado, for providing the code of the CCSM3. This study is supported by the National Centre of Competence in Research (NCCR) Climate funded by the Swiss National Science Foundation, the

European Commission Past4Future project (Grant 243908, 2010–14), and the Sinergia project FUPSOL. A.B. is supported by the European Commission under the Marie Curie Intra-European Fellowship ECLIPS (PIEF-GA-2011-300544). The simulations for this study were performed on a CRAY XT5 and XE6 at the Swiss National Supercomputing Centre (CSCS) in Lugano.

REFERENCES

Årthun, M., T. Eldevik, L. H. Smedsrud, O. Skagseth, and R. B. Ingvaldsen, 2012: Quantifying the influence of Atlantic heat on Barents Sea ice variability and retreat. *J. Climate,* **25,** 4736–4743.

Bauer, E., M. Claussen, and V. Brovkin, 2003: Assessing climate forcings of the Earth system for the past millennium. *Geophys. Res. Lett.,* **30,** 1276, doi:10.1029/2002GL016639.

Belkin, I., 2004: Propagation of the ''Great Salinity Anomaly'' of the 1990s around the northern North Atlantic. *Geophys. Res. Lett.,* **31,** L08306, doi:10.1029/2003GL019334.

Bengtsson, L., V. Semenov, and O. Johannessen, 2004: The early twentieth-century warming in the Arctic—A possible mechanism. *J. Climate,* **17,** 4045–4057.

Bitz, C., P. Gent, R. Woodgate, M. Holland, and R. Lindsay, 2006: The influence of sea ice on ocean heat uptake in response to increasing CO_2. *J. Climate,* **19,** 2437–2450.

Born, A., K. H. Nisancioglu, and P. Braconnot, 2010: Sea ice induced changes in ocean circulation during the Eemian. *Climate Dyn.,* **35** (7–8), 1361–1371, doi:10.1007/s00382-009-0709-2.

Bryan, F. O., G. Danabasoglu, N. Nakashiki, Y. Yoshida, D.-H. Kim, J. Tsutsui, and S. C. Doney, 2006: Response of the North Atlantic thermohaline circulation and ventilation to increasing carbon dioxide in CCSM3. *J. Climate,* **19,** 2382–2397.

Collins, W. D., and Coauthors, 2006: The Community Climate System Model version 3 (CCSM3). *J. Climate,* **19,** 2122–2143.

Cordero, E. C., and P. M. F. Forster, 2006: Stratospheric variability and trends in models used for the IPCC AR4. *Atmos. Chem. Phys.,* **6,** 5369–5380.

Crespin, E., H. Goosse, T. Fichefet, and M. E. Mann, 2009: The 15th century Arctic warming in coupled model simulations with data assimilation. *Climate Past,* **5,** 389–401.

Dickson, R. R., J. Meinke, S. A. Malmberg, and A. J. Lee, 1988: The ''Great Salinity Anomaly'' in the northern North Atlantic 1968–1982. *Prog. Oceanogr.,* **20,** 103–151, doi:10.1016/0079-6611(88)90049-3.

Goosse, H., and H. Renssen, 2002: Potential causes of abrupt climate events: A numerical study with a three-dimensional climate model. *Geophys. Res. Lett.,* **29,** 1860–1864.

Gray, L. J., and Coauthors, 2010: Solar influences on climate. *Rev. Geophys.,* **48,** RG4001, doi:10.1029/2009RG000282.

Häkkinen, S., 1999: A simulation of thermohaline effects of a great salinity anomaly. *J. Climate,* **12,** 1781–1795.

Hald, M., G. Salomonsen, K. Husum, and L. Wilson, 2011: A 2000 year record of Atlantic water temperature variability from the Malangen Fjord, northeastern North Atlantic. *Holocene,* **21,** 1049–1059.

Hofer, D., C. C. Raible, and T. F. Stocker, 2011: Variations of the Atlantic meridional overturning circulation in control and transient simulations of the last millennium. *Climate Past,* **7,** 133–150.

——, ——, A. Dehnert, and J. Kuhlemann, 2012a: The impact of different glacial boundary conditions on atmospheric dynamics and precipitation in the North Atlantic region. *Climate Past,* **8,** 935–949, doi:10.5194/cp-8-935-2012.

——, ——, N. Merz, A. Dehnert, and J. Kuhlemann, 2012b: Simulated winter circulation types in the North Atlantic and European region for preindustrial and glacial conditions. *Geophys. Res. Lett.,* **39,** L15805, doi:10.1029/2012GL052296.

Holland, M. M., C. M. Bitz, E. C. Hunke, W. H. Lipscomb, and J. L. Schramm, 2006: Influence of the sea ice thickness distribution on polar climate in CCSM3. *J. Climate,* **19,** 2398–2414.

Holliday, N. P., and Coauthors, 2008: Reversal of the 1960s to 1990s freshening trend in the northeast North Atlantic and Nordic Seas. *Geophys. Res. Lett.,* **35,** L03614, doi:10.1029/2007GL032675.

Hoskins, B. J., and D. J. Karoly, 1981: The steady linear response of a spherical atmosphere to thermal and orographic forcing. *J. Atmos. Sci.,* **38,** 1179–1196.

Houghton, J. T., and Coauthors, Eds., 2001: *Climate Change 2001: The Scientific Basis.* Cambridge University Press, 881 pp.

Ingvaldsen, R., L. Asplin, and H. Loeng, 2004: The seasonal cycle in the Atlantic transport to the Barents Sea during the years 1997–2001. *Cont. Shelf Res.,* **24,** 1015–1032, doi:10.1016/j.csr.2004.02.011.

Kinnard, C., C. M. Zdanowicz, D. A. Fisher, E. Isaksson, A. de Vernal, and L. G. Thompson, 2011: Reconstructed changes in Arctic sea ice over the past 1,450 years. *Nature,* **479,** 509–512, doi:10.1038/nature10581.

Knudsen, K. J., J. Eiríksson, and H. B. Bartels-Jónsdóttir, 2012: Oceanographic changes through the last millennium off north Iceland: Temperature and salinity reconstructions based on foraminifera and stable isotopes. *Mar. Micropaleontol.,* **84–85,** 54–73, doi:10.1016/j.marmicro.2011.11.002.

Kuhnert, H., and S. Mulitza, 2011: Multidecadal variability and late medieval cooling of near-coastal sea surface temperatures in the eastern tropical North Atlantic. *Paleoceanography,* **26,** PA4224, doi:10.1029/2011PA002130.

Lehner, F., C. C. Raible, and T. F. Stocker, 2012a: Testing the robustness of a precipitation proxy-based North Atlantic Oscillation reconstruction. *Quat. Sci. Rev.,* **45,** 85–94.

——, ——, ——, and D. Hofer, 2012b: The freshwater balance of polar regions in transient simulations from 1500 to 2100 AD using a comprehensive coupled climate model. *Climate Dyn.,* **39,** 347–363.

Li, C., D. S. Battisti, and C. M. Bitz, 2010: Can North Atlantic sea ice anomalies account for Dansgaard–Oeschger climate signals? *J. Climate,* **23,** 5457–5475.

Liu, Z., and Coauthors, 2009: Transient simulation of last deglaciation with a new mechanism for Bolling-Allerod warming. *Science,* **325** (5938), 310–314, doi:10.1126/science.1171041.

Mann, E. M., and Coauthors, 2009: Global signatures and dynamical origins of the Little Ice Age and Medieval Climate Anomaly. *Science,* **326,** 1256–1260, doi:10.1126/science.1177303.

Manzini, E., C. Cagnazzo, P. G. Fogli, A. Bellucci, and W. A. Mueller, 2012: Stratosphere-troposphere coupling at inter-decadal time scales: Implications for the North Atlantic Ocean. *Geophys. Res. Lett.,* **39,** L05801, doi:10.1029/2011GL050771.

Matthews, J., and K. R. Briffa, 2005: The 'Little Ice Age': Re-evaluation of an evolving concept. *Geogr. Ann.,* **87A,** 17–36, doi:10.1111/j.0435-3676.2005.00242.x.

Meehl, G., and Coauthors, 2006: Climate change projections for the twenty-first century and climate change commitment in the CCSM3. *J. Climate,* **19,** 2597–2616.

Miller, G. H., and Coauthors, 2012: Abrupt onset of the Little Ice Age triggered by volcanism and sustained by sea-ice/ocean feedbacks. *Geophys. Res. Lett.,* **39,** L02708, doi:10.1029/2011GL050168.

Otterå, O. H., M. Bentsen, H. Drange, and L. Suo, 2010: External forcing as a metronome for Atlantic multidecadal variability. *Nat. Geosci.,* **3,** 688–694, doi:10.1038/NGEO955.

Otto-Bliesner, B., R. Tomas, E. Brady, C. Ammann, Z. Kothavala, and G. Clauzet, 2006: Climate sensitivity of moderate- and low-resolution versions of CCSM3 to preindustrial forcings. *J. Climate,* **19,** 2567–2583.

Petoukhov, V., and V. A. Semenov, 2010: A link between reduced Barents-Kara sea ice and cold winter extremes over northern continents. *J. Geophys. Res.,* **115,** D21111, doi:10.1029/2009JD013568.

Pinto, J. G., and C. C. Raible, 2012: Past and recent changes in the North Atlantic Oscillation. *Wiley Interdiscip. Rev. Climate Change,* **3,** 79–90, doi:10.1002/wcc.150.

Schmidt, G. A., and Coauthors, 2012: Climate forcing reconstructions for use in PMIP simulations of the last millennium (v1.1). *Geosci. Model Dev.,* **5,** 185–191, doi:10.5194/gmd-5-185-2012.

Schröder, D., and W. M. Connolley, 2007: Impact of instantaneous sea ice removal in a coupled general circulation model. *Geophys. Res. Lett.,* **34,** L14502, doi:10.1029/2007GL030253.

Semenov, V. A., W. Park, and M. Latif, 2009: Barents Sea inflow shutdown: A new mechanism for rapid climate changes. *Geophys. Res. Lett.,* **36,** L14709, doi:10.1029/2009GL038911.

Shapiro, A. I., W. Schmutz, E. Rozanov, M. Schoell, M. Haberreiter, A. V. Shapiro, and S. Nyeki, 2011: A new approach to the long-term reconstruction of the solar irradiance leads to large historical solar forcing. *Astron. Astrophys.,* **529,** A67, doi:10.1051/0004-6361/201016173.

Solomon, S., D. Qin, M. Manning, Z. Chen, M. Marquis, K. B. Averyt, M. Tignor, and H. L. Miller Jr., Eds., 2007: *Climate Change 2007: The Science of Climate Change*. Cambridge University Press, 996 pp.

Spangehl, T., U. Cubasch, C. C. Raible, S. Schimanke, J. Körper, and D. Hofer, 2010: Transient climate simulations from the Maunder Minimum to present day: Role of the stratosphere. *J. Geophys. Res.,* **115,** D00I10, doi:10.1029/2009JD012358.

Spielhagen, R. F., and Coauthors, 2011: Enhanced modern heat transfer to the Arctic by warm Atlantic water. *Science,* **331,** 450–453, doi:10.1126/science.1197397.

Stocker, T. F., A. Timmermann, M. Renold, and O. Timm, 2007: Effects of salt compensation on the climate model response in simulations of large changes of the Atlantic meridional overturning circulation. *J. Climate,* **20,** 5912–5928.

Stouffer, R. J., and Coauthors, 2006: Investigating the causes of the response of the thermohaline circulation to past and future climate changes. *J. Climate,* **19,** 1365–1387.

Tietsche, S., D. Notz, J. H. Jungclaus, and J. Marotzke, 2011: Recovery mechanisms of Arctic summer sea ice. *Geophys. Res. Lett.,* **38,** L02707, doi:10.1029/2010GL045698.

Trouet, V., J. Esper, N. E. Graham, A. Baker, J. D. Scourse, and D. C. Frank, 2009: Persistent positive North Atlantic Oscillation mode dominated the Medieval Climate Anomaly. *Science,* **324,** 78–80, doi:10.1126/science.1166349.

——, J. D. Scourse, and C. C. Raible, 2012: North Atlantic storminess and Atlantic meridional overturning circulation during the last millennium: Reconciling contradictory proxy records of NAO variability. *Global Planet. Change,* **84–85,** 48–55, doi:10.1016/j.gloplacha.2011.10.003.

Wanamaker, A. D., Jr., P. G. Butler, J. D. Scourse, J. Heinemeier, J. Eiríksson, K. L. Knudsen, and C. A. Richardson, 2012: Surface changes in the North Atlantic meridional overturning circulation during the last millennium. *Nat. Commun.,* **3,** 899, doi:10.1038/ncomms1901.

Wanner, H., and Coauthors, 2008: Mid- to late Holocene climate change: An overview. *Quat. Sci. Rev.,* **27** (19–20), 1791–1828, doi:10.1016/j.quascirev.2008.06.013.

——, O. Solomina, M. Grosjean, S. P. Ritz, and M. Jetel, 2011: Structure and origin of Holocene cold events. *Quat. Sci. Rev.,* **30,** 3109–3123, doi:10.1016/j.quascirev.2011.07.010.

Wilmes, S. B., C. C. Raible, and T. F. Stocker, 2012: Climate variability of the mid- and high-latitudes of the Southern Hemisphere in ensemble simulations from 1500 to 2000 AD. *Climate Past,* **8,** 373–390, doi:10.5194/cp-8-373-2012.

Yiou, P., J. Servonnat, M. Yoshimori, D. Swingedouw, M. Khodri, and A. Abe-Ouchi, 2012: Stability of weather regimes during the last millennium from climate simulations. *Geophys. Res. Lett.,* **39,** L08703, doi:10.1029/2012GL051310.

Yoshimori, M., C. C. Raible, T. F. Stocker, and M. Renold, 2010: Simulated decadal oscillations of the Atlantic meridional overturning circulation in a cold climate state. *Climate Dyn.,* **34,** 101–121, doi:10.1007/s00382-009-0540-9.

Zanchettin, D., C. Timmreck, H.-F. Graf, A. Rubino, S. Lorenz, K. Lohmann, K. Krueger, and J. H. Jungclaus, 2012: Bi-decadal variability excited in the coupled ocean–atmosphere system by strong tropical volcanic eruptions. *Climate Dyn.,* **39** (1–2), 419–444, doi:10.1007/s00382-011-1167-1.

Zhong, Y., G. H. Miller, B. L. Otto-Bliesner, M. M. Holland, D. A. Bailey, D. P. Schneider, and A. Geirsdottir, 2011: Centennial-scale climate change from decadally-paced explosive volcanism: A coupled sea ice–ocean mechanism. *Climate Dyn.,* **37** (11–12), 2373–2387, doi:10.1007/s00382-010-0967-z.